A Simple Thermodynamic Model for Quantitatively Addressing Cooperativity in Multicomponent Self-Assembly Processes—Part 2: Extension to Multimetallic Helicates Possessing Different Binding Sites

Josef Hamacek,* Michal Borkovec, and Claude Piguet*[a]

Abstract: The extended site-binding model, which explicitly separates intramolecular interactions (i.e., intermetallic and interligand) from the successive binding of metal ions to polytopic receptors, is used for unravelling the self-assembly of trimetallic double-stranded Cu^{I} and triple-stranded Eu^{III} helicates. A thorough analysis of the available stability constants systematically shows that negatively cooperative processes operate, in strong contrast with previous reports invoking either statistical behaviours or positive cooperativity. Our results also highlight the need for combining successive generations of complexes with common binding units, but with increasing metallic nuclearities, for rationalizing and programming multicomponent supramolecular assemblies.

Keywords: cooperativity · helicate structures · lanthanides · thermodynamics

Introduction

In a previous contribution,[1] we have shown that the microscopic stability constant $\beta_{m,n}^{M,L}$ of a supramolecular complex $[M_m(L)_n]$ can be modeled with four parameters according to Equation (1).

$$\beta_{m,n}^{M,L} = \sigma_{chir}^{M,L}\omega_{m,n}\prod_{i=1}^{mn}(f_i^{M,L})\prod_{i=1}^{mn-m-n+1}(c_i^{eff})\prod_{i<j}{}''(u_{ij}^{MM})\prod_{k<l}{}'''(u_{kl}^{LL}) \quad (1)$$

In this equation $f_i^{M,L}$ represents the intermolecular microscopic affinity constant characterizing the connection of a metal M to the binding site i of a ligand L; $u_{ij}^{MM} = \exp(-\Delta E_{ij}^{MM}/RT)$ is the Boltzman's factor accounting for the intermetallic interaction ΔE_{ij}^{MM} (in term of free energy), which occurs when two metals occupy two adjacent binding sites i and j of the same ligand; $u_{kl}^{LL} = \exp(-\Delta E_{kl}^{LL}/RT)$ is the Boltzman's factor accounting for the interligand interactions ΔE_{kl}^{LL}, which results from the connection of two binding sites k and l to the same metal; and $c_i^{eff} = \exp((\Delta S_{i,intra}^{M,L} - \Delta S_{i,inter}^{M,L})/R)$ is the "effective concentration" used for correcting the entropy change observed between inter- and intramolecular binding processes. The term $\sigma_{chir}^{M,L}\omega_{m,n}$ represents the degeneracy of the microscopic state. For an achiral ligand **L*k***, $\sigma_{chir}^{M,L} = 1$, except when the point group of the $[M_m(L)_n]$ microspecies does not contain symmetry element of the second kind, then $\sigma_{chir}^{M,L} = 2$, and $\omega_{m,n}$ is evaluated for each microspecies by using standard statistical methods. Finally, the two last products $\prod''$ and $\prod'''$ run over all the pairs of adjacent intermetallic (u^{MM}) or interligand (u^{LL}) interactions occurring in the $[M_m(L)_n]$ microspecies.[1] Application of Equation (1) for modeling the formation of standard monometallic coordination complexes successfully reproduces experimental stability constants, and it further provides a quantitative analysis of the cooperativity (i.e., deviation from repetitive statistical binding) associated with the successive binding of ligands to a single metal.[1] Related mathematical analyses of the self-assembly of bimetallic triple-stranded helicates $[Eu_2(\mathbf{L}k)_3]$ ($k = 1$–3) is complicated by the various possible combinations of metals and ligands in the final complexes, and the fitting process fails for $k = 1$ or 2, because of the too limited sets of available experimental stability constants. For $[Eu_2(\mathbf{L3})_3]$, a sufficient amount of experimental data is accessible, and the use of Equation (1) eventually demonstrates that the assembly process is driven to completion by positive cooperativity, originating from attractive interligand interactions.[1]

[a] Dr. J. Hamacek, Prof. Dr. M. Borkovec, Prof. Dr. C. Piguet
Department of Inorganic, Analytical and Applied Chemistry
University of Geneva, 30 quai E. Ansermet
1211 Geneva 4 (Switzerland)
Fax: (+41) 22-379-68-30
E-mail: josef.hamacek@chiam.unige.ch
claude.piguet@chiam.unige.ch

Supporting information for this article is available on the WWW under http://www.chemeurj.org/ or from the author.

 DOI: 10.1002/chem.200500289 © 2005 Wiley-VCH Verlag GmbH & Co. KGaA, Weinheim

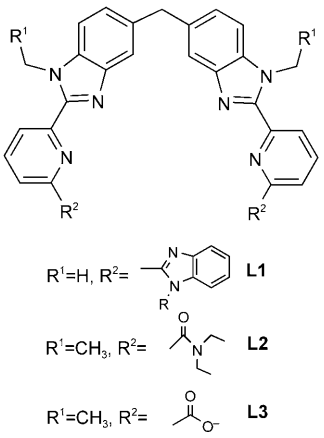

Although the extended site-binding model, mathematically formulated in Equation (1), has benefited from its application to basic complexation processes for its validation,[1] it is not limited to systems that display identical binding sites. It may apply, at least theoretically, to any multicomponent assembly process, and the famous self-assembly of Lehn's double-stranded trimetallic helicates $[Cu_3(\mathbf{Lk})_2]^{3+}$ ($k=4$, 5) plays a crucial role in this context, because 1) it involves (slightly) different binding sites along the strands, and 2) the associated thermodynamic constants have been originally interpreted within the frame of positive cooperativity according to Scatchard plots.[2,3] Interestingly, Ercolani recently pointed out that the latter approach did not take into account the entropy change occurring when a dative bound is part of a cyclic structure, and some corrective parameters, derived from the accepted theory of "effective concentration" used in macrocyclic chemistry, must be considered.[4] He indeed re-analysed the thermodynamic formation of $[Cu_3(\mathbf{L4})_2]^{3+}$ by using two thermodynamic microconstants K_{inter} and K_{intra}, which hold for the formation of inter- and intramolecular dative bonds, respectively. He eventually concluded that statistical binding occurs,[4] in contrast with the positively cooperative process originally suggested by Lehn.[2,3] However, Ercolani's model only considers the three first terms of Equation (1),[1] and it neglects the specific intramolecular interactions described by the last two terms. Therefore, the latter approach is only adequate, when both intramolecular interactions (intermetallic + interligand) are strictly proportional to the total number of bonds (mn) connecting the $m+n$ components in each $[M_m(L)_n]$ complex. Under these conditions, u^{MM} and u^{LL} can be safely partitioned and incorporated into K_{inter} and K_{intra}. However, this special case is rarely met in supramolecular chemistry,[5] and it does not hold for $[Eu_2(\mathbf{L3})_3]$.[1]

In this contribution, we propose a complete analysis of the archetypal thermodynamic self-assembly of $[Cu_3(\mathbf{Lk})_2]^{3+}$ ($k=4$, 5) with the help of Equation (1), which aims at unambiguously separating intramolecular interactions from repetitive statistical binding processes. A quantitative cooperativity index is then calculated for each complex participating to the assembly processes.[1] In the second section, Equation (1) is used for unravelling the assembly process of the more complicated trimetallic triple-stranded helicate $[Eu_3(\mathbf{L6})_3]^{9+}$, in which the central N_3 binding site is now significantly different from the terminal N_2O sites.[6–8] According to the considerable amount of parameters required for assigning a specific affinity to each binding site, the simultaneous fit of bimetallic $[Eu_2(\mathbf{Lk})_3]^{6+}$ ($k=1$, 2)[9,10] and trimetallic $[Eu_3(\mathbf{L6})_3]^{9+}$ complexes, containing common binding sites, is an attractive solution for reaching enough experimental data.

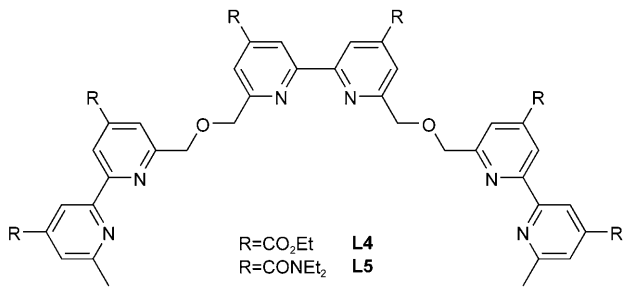

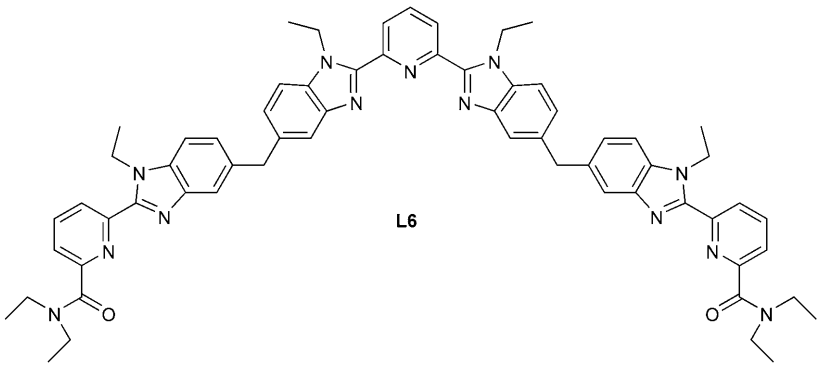

Results and Discussion

Application of the extended site-binding model to homotrimetallic helicates: The trimetallic helicates $[Cu_3(\mathbf{Lk})_2]^{3+}$ ($k=4$, 5) and $[Eu_3(\mathbf{L6})_3]^{9+}$ are obtained by the reaction of C_{2v}-symmetrical ligands **Lk** ($k=4$–6) with tetrahedral Cu^{I} (coordination number CN = 4),[2,3] or with tricapped trigonal prismatic Eu^{III} (CN = 9).[6,7] Each ligand **Lk** possesses

© 2005 Wiley-VCH Verlag GmbH & Co. KGaA, Weinheim

three adjacent binding segments ($p=3$), which are bidentate for **L4** and **L5** (denticity: dent = 2), and tridentate for **L6** (denticity: dent = 3). Consequently, the maximum valency v = CN/dent amounts to 4/2 = 2 for Cu^{I} in $[Cu_m(\mathbf{Lk})_n]^{m+}$ [k = 4, 5; m = 1–3, n = 1, 2, equilibrium in Eq. (2)], and to 9/3 = 3 for Eu^{III} in $[Eu_m(\mathbf{L6})_n]^{3m+}$ [m = 1–3, n = 1–3, equilibrium in Eq. (3)].

$$m\,Cu^{+} + n\,\mathbf{Lk} \rightleftharpoons [Cu_m(\mathbf{Lk})_n]^{m+} \qquad \beta_{m,n}^{Cu,\mathbf{Lk}} \qquad (2)$$

$$m\,Eu^{3+} + n\,\mathbf{L6} \rightleftharpoons [Eu_m(\mathbf{L6})_n]^{3m+} \qquad \beta_{m,n}^{Eu,\mathbf{L6}} \qquad (3)$$

Except for the different valencies v of the metals and the maximum number of ligands involved in the final complexes, the theoretical modeling of the formation constants depicted in the equilibria given in Equations (2) and (3) is identical, by means of Equation (1). Compared with **L1**–**L3**, which possess symmetry-related (i.e., equivalent) binding sites, the central binding site in **Lk** (k = 4–6) is different from the two appended terminal sites for evident symmetry reasons, and two different intermolecular microscopic affinity constants, adapted for the central $f_c^{M,\mathbf{Lk}}$ and terminal $f_t^{M,\mathbf{Lk}}$ sites, must be considered. Moreover, intermetallic interactions are no more limited to adjacent sites, and an additional long-range intermetallic interaction (u_t^{MM}) occurs between two metal ions lying in the terminal sites. A parallel behaviour affects the corrective effective concentration, and a novel term c_t^{eff}, accounting for microspecies in which only the well-separated terminal sites are occupied by metal ions, must be considered. The latter parameter is different from c^{eff}, which refers to the intramolecular connection between occupied adjacent sites, because the formation of smaller rings is entropically favoured (i.e., $c_t^{eff} < c^{eff}$).[4,11,12] Assuming the standard hypotheses characterizing helicate self-assemblies with semirigid ligand strands,[1,4,5] that is, 1) no hairpin structure is formed (two binding sites of the same ligand cannot bind to the same metal ion), 2) no constrained structure is formed (two terminal binding sites of the same ligand cannot connect to two adjacent metal ions borne by a second ligand), and 3) the principle of maximum site occupancy[13] is obeyed (as previously justified for $[Eu_2(\mathbf{L3})_3]$),[1] the application of Equation (1) with a single set of average effective concentrations (c^{eff}, c_t^{eff}), and interligand (u^{LL}) and intermetallic (u^{MM}, u_t^{MM}) interactions leads to the microscopic constants given in Equations (4)–(14) for double-stranded helicates, and Equations (4)–(21) for triple-stranded helicates, whereby the indices c and t refer to central and terminal sites, respectively. The schematic chemical structures associated with each microspecies are depicted in Figure 1.

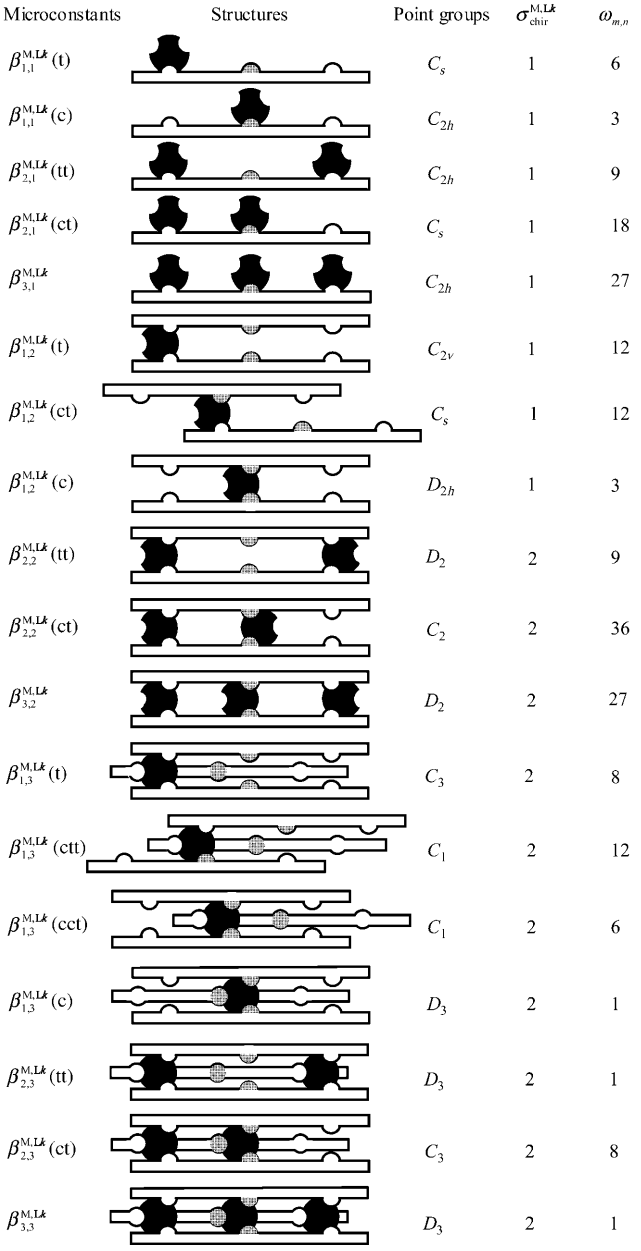

Figure 1. Arrangement of microspecies with three nonequivalent sites obeying the principle of maximum site occupancy. Schematic structures, symmetries and degeneracies of the $[M_m(\mathbf{Lk})_n]$ (m = 1–3, n = 1–3) microspecies described in the equilibria in Equations (2) and (3). The point groups are those established (or expected) in solution (^{1}H NMR spectroscopy, 298 K).[2,3,6,7]

$$\beta_{1,1}^{M,\mathbf{Lk}}(t) = \sigma_{chir,t}^{M,L}\omega_{1,1}^{t}(f_t^{M,\mathbf{Lk}}) \qquad (4)$$

$$\beta_{1,1}^{M,\mathbf{Lk}}(c) = \sigma_{chir,c}^{M,L}\omega_{1,1}^{c}(f_c^{M,\mathbf{Lk}}) \qquad (5)$$

$$\beta_{2,1}^{M,\mathbf{Lk}}(tt) = \sigma_{chir,tt}^{M,L}\omega_{2,1}^{tt}(f_t^{M,\mathbf{Lk}})^2(u_t^{MM}) \qquad (6)$$

$$\beta_{2,1}^{M,\mathbf{Lk}}(ct) = \sigma_{chir,ct}^{M,L}\omega_{2,1}^{ct}(f_t^{M,\mathbf{Lk}})(f_c^{M,\mathbf{Lk}})(u^{MM}) \qquad (7)$$

$$\beta_{3,1}^{M,\mathbf{Lk}} = \sigma_{chir}^{M,L}\omega_{3,1}(f_t^{M,\mathbf{Lk}})^2(f_c^{M,\mathbf{Lk}})(u^{MM})^2(u_t^{MM}) \qquad (8)$$

$$\beta_{1,2}^{M,\mathbf{Lk}}(t) = \sigma_{chir,t}^{M,L}\omega_{1,2}^{t}(f_t^{M,\mathbf{Lk}})^2(u^{LL}) \qquad (9)$$

$$\beta_{1,2}^{M,\mathbf{Lk}}(ct) = \sigma_{chir,ct}^{M,L}\omega_{1,2}^{ct}(f_c^{M,\mathbf{Lk}})(f_t^{M,\mathbf{Lk}})(u^{LL}) \qquad (10)$$

$$\beta_{1,2}^{M,\mathbf{Lk}}(c) = \sigma_{chir,c}^{M,L}\omega_{1,2}^{c}(f_c^{M,\mathbf{Lk}})^2(u^{LL}) \qquad (11)$$

$$\beta_{2,2}^{M,\mathbf{Lk}}(tt) = \sigma_{chir,tt}^{M,L}\omega_{2,2}^{tt}(f_t^{M,\mathbf{Lk}})^4(u^{LL})^2(u_t^{MM})(c_t^{eff}) \qquad (12)$$

 © 2005 Wiley-VCH Verlag GmbH & Co. KGaA, Weinheim

$$\beta_{2,2}^{M,Lk}(ct) = \sigma_{chir,ct}^{M,L}\omega_{2,2}^{ct}(f_t^{M,Lk})^2(f_c^{M,Lk})^2(u^{LL})^2(u^{MM})(c^{eff}) \quad (13)$$

$$\beta_{3,2}^{M,Lk} = \sigma_{chir}^{M,L}\omega_{3,2}(f_t^{M,Lk})^4(f_c^{M,Lk})^2(u^{LL})^3(u^{MM})^2(u_t^{MM})(c^{eff})^2 \quad (14)$$

$$\beta_{1,3}^{M,Lk}(t) = \sigma_{chir,t}^{M,L}\omega_{1,3}^{t}(f_t^{M,Lk})^3(u^{LL})^3 \quad (15)$$

$$\beta_{1,3}^{M,Lk}(ctt) = \sigma_{chir,ctt}^{M,L}\omega_{1,3}^{ctt}(f_t^{M,Lk})^2(f_c^{M,Lk})(u^{LL})^3 \quad (16)$$

$$\beta_{1,3}^{M,Lk}(cct) = \sigma_{chir,cct}^{M,L}\omega_{1,3}^{cct}(f_t^{M,Lk})(f_c^{M,Lk})^2(u^{LL})^3 \quad (17)$$

$$\beta_{1,3}^{M,Lk}(c) = \sigma_{chir,c}^{M,L}\omega_{1,3}^{c}(f_t^{M,Lk})^3(u^{LL})^3 \quad (18)$$

$$\beta_{2,3}^{M,Lk}(tt) = \sigma_{chir,tt}^{M,L}\omega_{2,3}^{tt}(f_t^{M,Lk})^6(u^{LL})^6(u_t^{MM})(c_t^{eff})^2 \quad (19)$$

$$\beta_{2,3}^{M,Lk}(ct) = \sigma_{chir,ct}^{M,L}\omega_{2,3}^{ct}(f_t^{M,Lk})^3(f_c^{M,Lk})^3(u_{LL})^6(u^{MM})(c^{eff})^2 \quad (20)$$

$$\beta_{3,3}^{M,Lk} = \sigma_{chir}^{M,L}\omega_{3,3}(f_t^{M,Lk})^6(f_c^{M,Lk})^3(u^{LL})^9(u^{MM})^2(u_t^{MM})(c^{eff})^4 \quad (21)$$

5) reduces to four $f^{M,Lk}$, u^{LL}, u^{MM} and c^{eff}, and a least-squares fit can be attempted with a minimum set of five experimental constants, which are available for $[Cu_m(\mathbf{L4})_n]^{m+}$ from thermodynamic[2] and kinetic[3] studies ($\beta_{1,1}^{Cu,L4}$, $\beta_{2,1}^{Cu,L4}$, $\beta_{1,2}^{Cu,L4}$, $\beta_{2,2}^{Cu,L4}$ and $\beta_{3,2}^{Cu,L4}$, Table 1). For $[Cu_m(\mathbf{L5})_n]^{m+}$, the more limited amount of available thermodynamic data (four constants, Table 1)[3] prevents the extraction of four independent microscopic parameters, and some of them must be, a priori, set to reasonable values provided by theoretical predictions.

The modeling of $[Cu_m(\mathbf{Lk})_n]^{m+}$ ($k=4$, 5; $m=1$–3, $n=1$, 2) thus relies on Equations (4)–(14), which involves the eleven possible microspecies depicted in Figure 2, because 1) the copper(I) valency amounts to $v=2$, and 2) the tris-bidentate ligand strands ($p=3$) possess two equivalent terminal sites ($p^t=2$) and one different central site ($p^c=1$), despite their similar microscopic affinities ($f_t^{Cu,Lk} \cong f_c^{Cu,Lk} = f^{Cu,Lk}$).

The least-squares fitting of the seven parameters, $f_c^{M,Lk}$, $f_t^{M,Lk}$, u^{LL}, u^{MM}, u_t^{MM}, c^{eff}, and c_t^{eff} requires at least eight experimental macroscopic constants, which are not yet available for any self-assembly process.

Modeling the self-assembly of double-stranded helicates $[Cu_m(Lk)_n]^{m+}$ ($k=4$, 5): Although not equivalent, the terminal and central bipyridine sites in **L4**, or in **L5**, are very similar and the approximation $f_t^{Cu,Lk} \cong f_c^{Cu,Lk} = f^{Cu,Lk}$ is justified for these ligands, because comparable stability constants are found for the complexes formed by 4,4′-diethylcarboxy-6,6′-dimethyl-2,2′-bipyridine, or 4,4′-*N*,*N*′-diethylcarboxamido-6,6′-dimethyl-2,2′-bipyridine with Cu^I.[3] Moreover, the distance between two linked binding sites (r) can be reliably approximated by the intermetallic distances found in the crystal structures of these multimetallic helicates, which show that the separation between the central and terminal sites ($r_{ct}=5.8$ Å) is half that measured between the two terminal sites ($r_{tt}=2r_{ct}$).[3b] Since both u^{MM} and c^{eff} depend on r, according to $u^{MM} \propto e^{1/r}$,[8] and $c^{eff} \propto 1/r^3$,[14,15] the parameters u_t^{MM} and c_t^{eff} can be modeled with $u_t^{MM} = (u^{MM})^{0.5}$ and $c_t^{eff} = c^{eff}/8$, respectively. As discussed in the theoretical part,[1] the dependence of c^{eff} may deviate from r^{-3} for rigid systems, in which the second binding site cannot access the volume of a whole sphere (i.e., for an access limited to the surface of a sphere, a r^{-2} dependence is expected).[14,15] However, the oxopropylene spacers in **L4** and **L5**, ensure enough flexibility for limiting significant deviations from the asymptotic r^{-3} dependence. With these reasonable approximations, the number of parameters required for modeling the formation of $[Cu_m(\mathbf{Lk})_n]^{m+}$ ($k=4$,

Table 1. Experimental and fitted[a] stability constants for $[Cu_m(\mathbf{L4})_n]^{m+}$ (acetonitrile/dichloromethane 1:1, 298 K) and $[Cu_m(\mathbf{L5})_n]^{m+}$ complexes (acetonitrile/water/dichloromethane 80:15:5, 298 K).

Species	L = **L4**			L = **L5**		
	$\log(\beta_{m,n}^{Cu,L4})$ (exptl)	$\log(\beta_{m,n}^{Cu,L4})$ model 1[b]	$\log(\beta_{m,n}^{Cu,L4})$ model 2[c]	$\log(\beta_{m,n}^{Cu,L5})$ (exptl)	$\log(\beta_{m,n}^{Cu,L5})$ model 1[d]	$\log(\beta_{m,n}^{Cu,L5})$ model 2[e]
$[CuLk]^+$	4.0(5)[f]	4.7	4.5	3.6(4)[f]	4.6	3.9
$[Cu_2Lk]^{2+}$	8.0(5)	7.7	7.8	8.1(3)	7.6	8.0
$[Cu_3Lk]^{3+}$	–	8.1	9.8	–	8.7	[g]
$[Cu(Lk)_2]^+$	8.2(2)	8.0	7.9	–	5.9	6.6
$[Cu_2(Lk)_2]^{2+}$	13.5(2)	13.9	13.7	12.9(3)	12.9	12.7
$[Cu_3(Lk)_2]^{3+}$	18.6(1)	18.4	18.6	18.7(3)	18.7	18.8

[a] Computed using the fitted parameters in Table 2 and Equations (22)–(27). The quoted errors correspond to those reported in reference [3]. [b] $\log(u^{MM}) = -1.8$. [c] $c^{eff} = 1.3$. [d] $\log(u^{MM}) = -1.4$. [e] $c^{eff} = 1.3$. [f] The thermodynamic stability constants obtained for $[CuLk]^+$ ($k=4$, 5) correspond to hairpin structures,[3] while the alternative stability constants determined from kinetic data, as mentioned in Table 1, refer to linear arrangements, in which Cu^I is coordinated by a single bipyridine group.[3] [g] Reliable predictions for multimetallic complexes not included in the fitting process cannot be obtained with this model, because $\log(u^{MM}) > 0$ (Table 2).

We have previously demonstrated[1] that the total degeneracy of a macrospecies $[M_m(Lk)_n]$ possessing n ligand strands with p symmetry-related (i.e., equivalent) binding sites is given by $\omega_{m,n}(\text{macro}) = (C_n^v)^m(C_m^p)^n$, whereby the binomial coefficients C_n^v stand for the number of ways of putting n ligands to v positions available around one metal ion ($n \leq v$), and C_m^p refers to the number of ways of connecting m metals to the available p binding sites of one ligand ($m \leq p$).[1] When different sites are available within the strand, the latter calculation only holds for complexes in which all the binding sites are occupied by metals ($m=p$), a situation encountered for $[Cu_3(Lk)]^{3+}$ ($\omega_{3,1} = (C_1^2)^3(C_3^3)^1 = 8$) and $[Cu_3(Lk)_2]^{3+}$ ($\omega_{3,2} = (C_2^2)^3(C_3^3)^1 = 1$, Figure 2). However, for complexes with partially occupied binding sites ($m<p$), the macroscopic degeneracy is partitioned between several contributing microspecies possessing different energies. Since we consider that interligand (u^{LL}) and intermetallic (u^{MM}) interactions do not depend on the specific structure of the complexes, each $[Cu_m(Lk)_n]^{m+}$ macrospecies, for which $m<p$, is made up of $n+1$ different microspecies. The degenera-

© 2005 Wiley-VCH Verlag GmbH & Co. KGaA, Weinheim

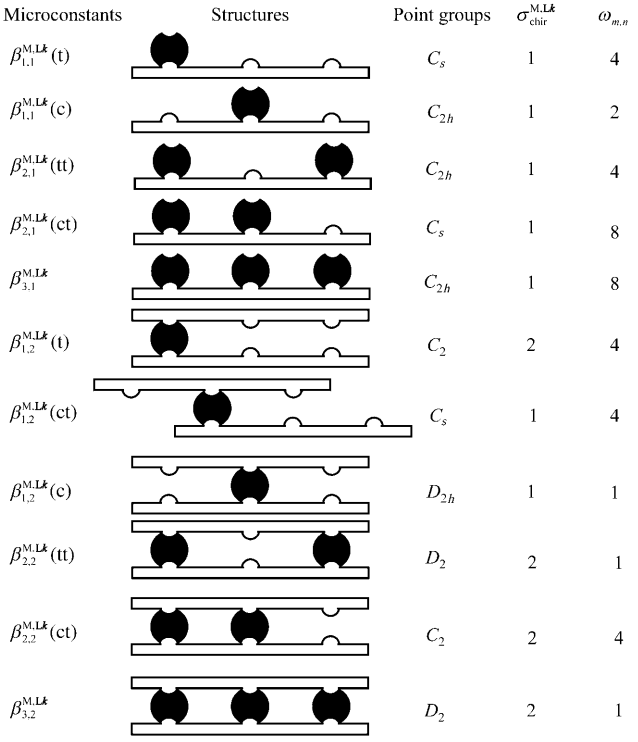

Figure 2. Arrangement of microspecies in $[Cu_m(\mathbf{Lk})_n]^{m+}$ ($k=4$, 5) obeying the principle of maximum site occupancy. Schematic structures, symmetries and degeneracies of the $[Cu_m(\mathbf{Lk})_n]^{m+}$ microspecies described in the equilibrium given in Equation (2) ($k=4$, 5). The point groups are those established (or expected) in solution (^{1}H NMR spectroscopy, 298 K).[3]

cy of each microspecies is calculated in the appendix and is summarized in Figure 2, while the associated microconstants computed with Equations (4)–(14) are combined to give the macroconstants in Equations (22)–(27).

$$\beta_{1,1}^{Cu,\mathbf{Lk}} = 6(f^{Cu,\mathbf{Lk}}) \quad (22)$$

$$\beta_{2,1}^{Cu,\mathbf{Lk}} = 4(f^{Cu,\mathbf{Lk}})^2(u^{MM})^{0.5} + 8(f^{Cu,\mathbf{Lk}})^2(u^{MM}) \quad (23)$$

$$\beta_{3,1}^{Cu,\mathbf{Lk}} = 8(f^{Cu,\mathbf{Lk}})^3(u^{MM})^{2.5} \quad (24)$$

$$\beta_{1,2}^{Cu,\mathbf{Lk}} = 13(f^{Cu,\mathbf{Lk}})^2(u^{LL}) \quad (25)$$

$$\beta_{2,2}^{Cu,\mathbf{Lk}} = 2(f^{Cu,\mathbf{Lk}})^4(u^{LL})^2(u^{MM})^{0.5}(c^{eff}/8) + 8(f^{Cu,\mathbf{Lk}})^4(u^{LL})^2(u^{MM})(c^{eff}) \quad (26)$$

$$\beta_{3,2}^{Cu,\mathbf{Lk}} = 2(f^{Cu,\mathbf{Lk}})^6(u^{LL})^3(u^{MM})^{2.5}(c^{eff})^2 \quad (27)$$

A nonlinear least-squares fit of the four parameters $f^{M,\mathbf{Lk}}$, c^{eff}, u^{MM}, and u^{LL} for $[Cu_m(\mathbf{L4})_n]^{m+}$ by using Equations (22), (23), and (25)–(27) (corresponding to the available experimental macroconstants collected in Table 1) provides an almost ideal match between experimental and computed formation constants, but the resulting large negative value of ΔE^{MM} cannot account for the expected repulsion between two cations coordinated to the neutral ligands. This strongly suggests that our set of only five equations is not sufficient for extracting four independent parameters. Therefore, we decided to fix either 1) $\log(u^{MM})$ in model 1 {calculated for the electrostatic repulsion[8] between two adjacent monocationic Cu^I ions separated by 5.8 Å[2,3] in acetonitrile/dichloromethane 1:1 ($\varepsilon_r \sim 23$) for $[Cu_m(\mathbf{L4})_n]^{m+}$ ($\log(u^{MM}) = -1.8$),[2] or in acetonitrile/water/dichloromethane ($\varepsilon_r \sim 30$) for $[Cu_m(\mathbf{L5})_n]^{m+}$($\log(u^{MM}) = -1.4$)},[3] or 2) $c^{eff} = 1.3$ in model 2 (calculated for a single-stranded flexible polymer in which the adjacent binding sites are separated by 5.8 Å).[14] All fits converge to a unique microscopic intermolecular free energy of connection $\Delta g_{inter}^{Cu,\mathbf{Lk}} \approx -21$ kJ mol^{-1} for the binding (including desolvation) of Cu^I to a substituted bipyridine site found in Cu–**L*k*** systems ($k=4$, 5, Table 2). As expected, the replacement of ester substituents (**L4**) with amides (**L5**) has negligible effects on the affinity for Cu^I.[2,3] A slightly repulsive interligand interaction $\Delta E^{LL} \approx 5$ kJ mol^{-1} (Table 2) is found for both **L4** and **L5** ligands, which can be tentatively assigned to the steric congestion resulting from the wrapping of the strands around small Cu^I metal ions, a phenomenon responsible for the extremely slow twisting observed by kinetics.[3] However, the large uncertainties affecting the fitted ΔE^{LL} parameter suggest that deviation from statistics (i.e., $\Delta E^{LL} = 0$) remains moderate. We also note that u^{MM} and c^{eff} are correlated because of the two small sets of available macroscopic thermodynamic constants. When u^{MM} is fixed (model 1), the fitted c^{eff} parameter displays large uncertainties, which prevents detailed interpretation (Table 2). The reverse situation is found when c^{eff} is fixed (model 2, Table 2). However, the macroscopic stability constants computed for the Cu–**L*k*** complexes with both models are in a fair agreement with experimental data (Table 1), which 1) supports our model despite the only limited amount of thermodynamic data and 2) allows an estimation for the stability constants of $[Cu_3\mathbf{Lk}]^{3+}$ ($k=4$, 5) ($\beta_{3,1}^{Cu,\mathbf{L5}} = 8$–10) and $[Cu(\mathbf{L5})_2]^+$ ($\beta_{1,2}^{Cu,\mathbf{L5}} = 6$–7), for which no experimental formation constants are available. We also note that the accuracy of the recalculated constants $\beta_{1,2}^{Cu,\mathbf{L4}}$, $\beta_{2,2}^{Cu,\mathbf{L4}}$, and $\beta_{3,2}^{Cu,\mathbf{L4}}$ is com-

Table 2. Fitted thermodynamic parameters for $[Cu_m(\mathbf{L4})_n]^{m+}$ (acetonitrile/dichloromethane 1:1, 298 K) and $[Cu_m(\mathbf{L5})_n]^{m+}$ complexes (acetonitrile/water/dichloromethane 80:15:5, 298 K).[a]

Fitted parameters	$[Cu_m(\mathbf{L4})_n]^{m+}$ model 1[b]	$[Cu_m(\mathbf{L4})_n]^{m+}$ model 2[c]	$[Cu_m(\mathbf{L5})_n]^{m+}$ model 1[d]	$[Cu_m(\mathbf{L5})_n]^{m+}$ model 2[e]
$\log(f^{Cu,\mathbf{Lk}})/\Delta g_{inter}^{Cu,\mathbf{Lk}}$ [kJ mol^{-1}]	3.9(3)/−22(2)	3.7(2)/−21(1)	3.8(5)/−22(3)	3.1(3)/−18(2)
$\log(u^{LL})/\Delta E^{LL}$ [kJ mol^{-1}]	−1.0(9)/6(5)	−0.6(4)/4(2)	−2.8(2.6)/16(15)	−0.7(4)/4(2)
$\log(u^{MM})/\Delta E^{MM}$ [kJ mol^{-1}]	−1.8/10.4	−0.9(5)/5(3)	−1.4/7.0	0.8(6)/−4(3)
$\log(c^{eff})/\Delta g_{corr}^{Cu,\mathbf{Lk}}$ [kJ mol^{-1}]	1(1)/−6(6)	0.11/−0.65	4(4)/−22(22)	0.11/−0.65

[a] The calculated values of $\log(u^{MM})$ or c^{eff} were blocked during the fitting process (see text). Standard errors estimated by the least-squares fits are given between parentheses. [b] $\log(u^{MM}) = -1.8$. [c] $c^{eff} = 1.3$. [d] $\log(u^{MM}) = -1.4$. [e] $c^{eff} = 1.3$.

 © 2005 Wiley-VCH Verlag GmbH & Co. KGaA, Weinheim

parable with that observed when using Ercolani's model,[4] which only considers the three first terms of Equation (1). This situation results from the approximate proportional correlation between the number of intramolecular interactions (interligand and intermetallic) and the total number of metal–ligand connections within the incriminated complexes $[Cu_m(\mathbf{Lk})_n]^{m+}$ in Equations (25)–(27). However, the parameters describing these intramolecular interactions are included within the microscopic constants K_{inter} and K_{intra} in the latter model, which prevents a rational assessment of cooperativity.

As previously discussed, the two last terms of Equation (1) indeed combine any deviations from statistical behaviour, and partial (I_c^{MM}, I_c^{LL}) and global (I_c^{tot}) cooperativity indexes can be thus calculated with Equation (28).[1] Taking the specific mathematical development for the $\prod''$ and $\prod'''$ products of each $[Cu_m(\mathbf{Lk})_n]^{m+}$ microspecies described in Equations (22)–(27), leads to the cooperativity indexes collected in Table 3.

Table 3. Indexes of cooperativity (I_c) for the formation of the microspecies $[Cu_m(\mathbf{L4})_n]^{m+}$ [a], $[Cu_m(\mathbf{L5})_n]^{m+}$ [a] and $[Eu_m(\mathbf{Lk})_n]^{3m+}$($k=1$, 2, 6).

Microspecies	$\log(I_c^{LL})$ (ΔE_c^{LL})[b]	$\log(I_c^{MM})$ (ΔE_c^{MM})[b]	$\log(I_c^{tot})$ (ΔE_c^{tot})[b]	Cooperativity
$[Cu_2\mathbf{L4}]^{2+}$ (ct)	–	−1.8 (10)	−1.8 (10)	negative
$[Cu_2\mathbf{L4}]^{2+}$ (tt)	–	−0.9 (5.0)	−0.9 (5.0)	negative
$[Cu(\mathbf{L4})_2]^{+}$ (t)	−1.0 (5.6)	–	−1.0 (5.6)	negative
$[Cu(\mathbf{L4})_2]^{+}$ (ct)	−1.0 (5.6)	–	−1.0 (5.6)	negative
$[Cu_2(\mathbf{L4})_2]^{2+}$ (ct)	−2.0 (11)	−1.8 (10)	−3.8 (21)	negative
$[Cu_2(\mathbf{L4})_2]^{2+}$ (tt)	−2.0 (11)	−0.9 (5.0)	−2.9 (16)	negative
$[Cu_3(\mathbf{L4})_2]^{3+}$	−3.0(17)	−4.5 (26)	−7.5 (43)	negative
$[Cu_2\mathbf{L5}]^{2+}$ (ct)	–	−1.4 (8.0)	−1.4 (8.0)	negative
$[Cu_2\mathbf{L5}]^{2+}$ (tt)	–	−0.7 (4.0)	−0.7 (4.0)	negative
$[Cu_2(\mathbf{L5})_2]^{2+}$ (ct)	−5.6 (32)	−1.4 (8.0)	−7.0 (40)	negative
$[Cu_2(\mathbf{L5})_2]^{2+}$ (tt)	−5.6 (32)	−0.7 (4.0)	−6.3 (36)	negative
$[Cu_3(\mathbf{L5})_2]^{3+}$	−8.4 (48)	−3.5 (20)	−11.9 (68)	negative
$[Eu_2(\mathbf{L6})_3]^{6+}$ (ct)	−16.2 (92)	−6.7 (38)	−22.9 (130)	negative
$[Eu_2(\mathbf{L6})_3]^{6+}$ (tt)	−16.2 (92)	−3.3 (19)	−19.5 (111)	negative
$[Eu_3(\mathbf{L6})_2]^{9+}$	−8.1 (46)	−16.7 (95)	−24.8 (141)	negative
$[Eu_3(\mathbf{L6})_3]^{9+}$	−24.2 (138)	−16.7 (95)	−40.9 (233)	negative
$[Eu(\mathbf{L1})_2]^{3+}$	−2.7 (15)	–	−2.7 (15)	negative
$[Eu(\mathbf{L2})_3]^{3+}$	−8.1 (46)	–	−8.1 (46)	negative
$[Eu_2(\mathbf{Lk})_2]^{6+}$	−5.4 (31)	−6.7 (38)	−12.1 (69)	negative
$[Eu_2(\mathbf{Lk})_3]^{6+}$	−16.2 (92)	−6.7 (38)	−22.8 (130)	negative

[a] Computed using the fitted parameters in Table 2 with fixed intermetallic interactions ($\log(u^{MM})=-1.8$ (**L4**) or −1.4 (**L5**)). [b] Cooperativity indexes calculated with Equation (28).[1] Values in kJ mol^{-1} are given between parentheses.

$$I_c^{tot} = I_c^{MM} I_c^{LL} = \prod_{i<j}{}''(u_{ij}^{MM}) \prod_{k<l}{}'''(u_{kl}^{LL}) \qquad (28)$$

Systematic negatively cooperative behavior is evidenced, because both interligand ($I_c^{LL}<1$) and intermetallic ($I_c^{MM}<1$) interactions are repulsive in these assembly processes. However, the free energy difference between two cooperative indexes calculated for $[Cu_m(\mathbf{Lk})_n]^{m+}$ complexes displaying identical global complexities $GC=m+n$, is relatively small (Table 3), which implies that both reaction pathways involving $[Cu_2\mathbf{Lk}]^{2+}$ or $[Cu(\mathbf{Lk})_2]^{+}$ may compete for the formation of the final helicate, a behaviour indeed observed by kinetics.[3] In the same context, the estimation of a strong negatively cooperative index for $[Cu_3\mathbf{Lk}]^{3+}$ ($\Delta E_c^{tot}=20$–26 kJ mol^{-1}, Table S1, Supporting Information) justifies that thermodynamics drives the reaction by means of the $[Cu_2(\mathbf{Lk})_2]^{2+}$ pathway, in complete agreement with the non-detection of $[Cu_3\mathbf{Lk}]^{3+}$ during the kinetic studies.[3]

Modeling the self-assembly of triple-stranded helicates $[Eu_m(\mathbf{L6})_n]^{3m+}$: For lanthanide complexes with the ligand **L6** [equilibrium given in Eq. (3)], the assumption of similar affinities for the central (N_3) and the terminal (N_2O) binding sites is not adequate, and two different intermolecular microscopic affinity constants $f_c^{M,\mathbf{Lk}}$ and $f_t^{M,\mathbf{Lk}}$ must be considered. On the other hand, since the distance between the terminal sites is still twice that between adjacent sites,[6] the parameterization $u_t^{MM}=(u^{MM})^{1/2}$, and $c_t^{eff}=c^{eff}/8$, still holds. Moreover, the degeneracy of each macrospecies $\omega_{m,n}(\text{macro})=(C_n^v)^m(C_m^p)^n$ is partitioned between $n+1$ different contributing microspecies ($m<p$), specific degeneracies of which are calculated with Equation (45) (see Appendix), reminding that $v=3$ and $p=3$, together with $p^t=2$ and $p^c=1$ for $[Eu_m(\mathbf{L6})_n]^{3m+}$. The computed degeneracies for the eighteen possible microspecies [Eqs. (4)–(21)] matching the structural criteria used in helicate self-assembly (i.e., no hairpin or constrained structures, and maximum occupancy of the sites), are collected in Figure 1. Combination of the microconstants possessing identical stoichiometries, leads to the macroconstants given in Equations (29)–(37) for $[Eu_m(\mathbf{L6})_n]^{3m+}$. However, only three experimental macroscopic constants are available ($\beta_{3,2}^{Ln,\mathbf{L6}}$, $\beta_{2,3}^{Ln,\mathbf{L6}}$, and $\beta_{3,3}^{Ln,\mathbf{L6}}$)[6] for fitting five parameters $f_t^{M,\mathbf{Lk}}$, $f_c^{M,\mathbf{Lk}}$, u^{MM}, u^{LL}, c^{eff}, which prevents a direct modeling.

$$\beta_{1,1}^{Eu,\mathbf{Lk}} = 6(f_t^{M,\mathbf{Lk}}) + 3(f_c^{M,\mathbf{Lk}}) \qquad (29)$$

$$\beta_{2,1}^{Eu,\mathbf{Lk}} = 9(f_t^{M,\mathbf{Lk}})^2(u^{MM})^{0.5} + 18(f_c^{M,\mathbf{Lk}})(f_t^{M,\mathbf{Lk}})(u^{MM}) \qquad (30)$$

$$\beta_{3,1}^{Eu,\mathbf{Lk}} = 27(f_t^{M,\mathbf{Lk}})^2(f_c^{M,\mathbf{Lk}})(u^{MM})^{2.5} \qquad (31)$$

$$\beta_{1,2}^{Eu,\mathbf{Lk}} = 3(u^{LL})[4(f_t^{M,\mathbf{Lk}})^2 + 4(f_c^{M,\mathbf{Lk}})(f_t^{M,\mathbf{Lk}}) + 1(f_c^{M,\mathbf{Lk}})^2] \qquad (32)$$

$$\beta_{2,2}^{Eu,\mathbf{Lk}} = 18(u^{LL})^2[(f_t^{M,\mathbf{Lk}})^4(u_t^{MM})^{0.5}(c^{eff}/8) + 4(f_c^{M,\mathbf{Lk}})^2(f_t^{M,\mathbf{Lk}})^2(u^{MM})(c^{eff})] \qquad (33)$$

© 2005 Wiley-VCH Verlag GmbH & Co. KGaA, Weinheim

$$\beta_{3,2}^{Eu,\mathbf{Lk}} = 54(u^{LL})^3(f_c^{M,\mathbf{Lk}})^2(f_t^{M,\mathbf{Lk}})^4(u^{MM})^{2.5}(c^{eff})^2 \quad (34)$$

$$\beta_{1,3}^{Eu,\mathbf{Lk}} = 2(u^{LL})^3[8(f_t^{M,\mathbf{Lk}})^3 + 12(f_t^{M,\mathbf{Lk}})^2(f_c^{M,\mathbf{Lk}}) + 6(f_t^{M,\mathbf{Lk}})(f_c^{M,\mathbf{Lk}})^2 + (f_c^{M,\mathbf{Lk}})^3] \quad (35)$$

$$\beta_{2,3}^{Eu,\mathbf{Lk}} = 2(u^{LL})^6[(f_t^{M,\mathbf{Lk}})^6(u^{MM})^{0.5}(c^{eff}/8)^2 + 8(f_t^{M,\mathbf{Lk}})^3(f_c^{M,\mathbf{Lk}})^3(u^{MM})(c^{eff})^2] \quad (36)$$

$$\beta_{3,3}^{Eu,\mathbf{Lk}} = 2(u^{LL})^9(f_t^{M,\mathbf{Lk}})^6(f_c^{M,\mathbf{Lk}})^3(u^{MM})^{2.5}(c^{eff})^4 \quad (37)$$

To increase the number of available equations, for which the experimental formation constants are accessible, we reasonably assume that the central tridentate N_3 binding unit in **L6** is identical to those found in **L1**, while the terminal tridentate N_2O binding units are common for **L6** and **L2**. Moreover, the intermetallic separation is similar ($\approx$9 Å) for all complexes due to the use of a unique rigid diphenylmethane spacer in **Lk** (k=1, 2, 6).[6,8] In these conditions, we can consider a single set of five parameters $f_{N_3}^{Eu}$, $f_{N_2O}^{Eu}$, u^{MM}, u^{LL}, and c^{eff} for simultaneously fitting the nine experimental formation constants described in Equations (34), (36), and (37) for $[Eu_m(\mathbf{L6})_n]^{3m+}$,[6] and Equations (38)–(43)[1] for $[Eu_m(\mathbf{Lk})_n]^{3m+}$ (k=1, 2).[8–10]

$$\beta_{1,2}^{Eu,\mathbf{L1}} = 12(f_{N_3}^{Eu})^2(u^{LL}) \quad (38)$$

$$\beta_{2,2}^{Eu,\mathbf{L1}} = 9(f_{N_3}^{Eu})^4(u^{LL})^2(u^{MM})(c^{eff}) \quad (39)$$

$$\beta_{2,3}^{Eu,\mathbf{L1}} = 2(f_{N_3}^{Eu})^6(u^{LL})^6(u^{MM})(c^{eff})^2 \quad (40)$$

$$\beta_{1,3}^{Eu,\mathbf{L2}} = 16(f_{N_2O}^{Eu})^3(u^{LL})^3 \quad (41)$$

$$\beta_{2,2}^{Eu,\mathbf{L2}} = 9(f_{N_2O}^{Eu})^4(u^{LL})^2(u^{MM})(c^{eff}) \quad (42)$$

$$\beta_{2,3}^{Eu,\mathbf{L2}} = 2(f_{N_2O}^{Eu})^6(u^{LL})^6(u^{MM})(c^{eff})^2 \quad (43)$$

Due to the rather large uncertainties affecting some formation constants (Table 4, vide supra), combined with significant correlations between the fitted parameters, we included two additional restraints in the nonlinear least-squares fitting process. 1) The maximum acceptable intermetallic interaction corresponds to the electrostatic repulsion calculated between two triply charged cations separated by 9 Å in $[Eu_m(\mathbf{Lk})_n]^{3m+}$ ($\varepsilon_r \approx 30$, $\Delta E^{MM} \leq 48\ kJ\,mol^{-1}$, $\log(u^{MM}) \geq -8.4$).[8] 2) The minimum acceptable effective concentration corresponds to that expected for two adjacent sites separated by 9 Å in a single-stranded polymer ($c^{eff} \geq 0.34$),[14] because the increased rigidity and preorganization in the multistranded $[Eu_m(\mathbf{Lk})_n]^{3m+}$ assemblies favor intramolecular cyclization over intermolecular complexation (i.e., $R\ln(c^{eff}) = \Delta S_{intra} - \Delta S_{inter}$ becomes larger).[1,15] In these conditions the global nonlinear least-squares fit of Equations (34) and (36)–(43) converges to the set of $f_{N_3}^{Eu}$, $f_{N_2O}^{Eu}$, u^{MM}, u^{LL}, and c^{eff} parameters collected in Table 5, which produces recalculated stability constants in fair agreement with experimental data, except for $[Eu(\mathbf{L2})_3]^{3+}$ (Table 4, Figure 3). For the self-assemblies of $[Cu_m(\mathbf{Lk})_n]^{m+}$ and $[Eu_m(\mathbf{Lk})_n]^{3m+}$, the experimental formation constants are obtained by direct spectrophotometric titrations; this strongly limits their accuracy because the quantities of free ligands and metals are negligible

Table 4. Experimental and fitted stability constants for $[Eu_m(\mathbf{Lk})_n]^{3m+}$ (k=1, 2, 6) (simultaneous fits, acetonitrile, 298 K).[a]

Species	$\log(\beta_{m,n}^{Eu,\mathbf{Lk}})$ (exptl)	$\log(\beta_{m,n}^{Eu,\mathbf{Lk}})$ (calcd) global fit	$\log(\beta_{m,n}^{Eu,\mathbf{Lk}})$ (calcd) model 1[b]	$\log(\beta_{m,n}^{Eu,\mathbf{Lk}})$ (calcd) model 2[c]
$[Eu(\mathbf{L1})_2]^{3+}$	11.6(3)	12.6	13.1	11.9
$[Eu_2(\mathbf{L1})_2]^{6+}$	18.1(3)	19.3	19.4	18.3
$[Eu_2(\mathbf{L1})_3]^{6+}$	24.3(4)	24.2	24.5	24.2
$[Eu(\mathbf{L2})_3]^{3+}$	19.4(5)	15.6	15.9	16.8
$[Eu_2(\mathbf{L2})_2]^{6+}$	19.6(2)	20.9	20.9	20.0
$[Eu_2(\mathbf{L2})_3]^{6+}$	26.0(2)	26.5	26.8	26.8
$[Eu_2(\mathbf{L6})_3]^{6+}$	25.9(1.4)	28.1	29.1	27.0
$[Eu_3(\mathbf{L6})_2]^{9+}$	26.0(1.6)	25.3	23.8	25.5
$[Eu_3(\mathbf{L6})_3]^{9+}$	34.8(1.6)	33.9	33.2	34.5

[a] Computed using the fitted parameters in Table 5 and Equations (34) and (36)–(43). The quoted errors correspond to those reported by authors in references [6,8] and [10]. [b] $\log(u^{MM}) = -8.4$. [c] $c^{eff} = 0.34$.

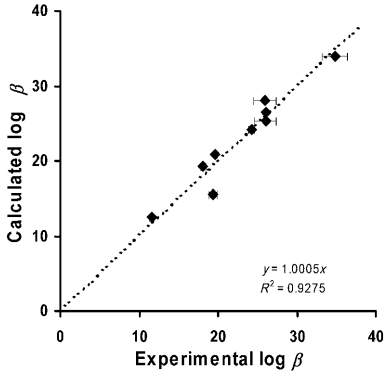

Figure 3. Correlation between experimental and calculated stability constants for $[Eu_m(\mathbf{Lk})_n]^{3m+}$ (k=1, 2, 6) (global fit, acetonitrile, 298 K). Error bars correspond to those obtained during the nonlinear least-squares fits of the spectrophotometric data (see text).

Table 5. Fitted thermodynamic parameters for $[Eu_m(\mathbf{Lk})_n]^{3m+}$ (k=1, 2, 6) (simultaneous fits, acetonitrile, 298 K).

Fitted parameters	global fit	model 1[a,b]	model 2[a,c]
$\log(f_{N_3}^{Eu,\mathbf{Lk}})/\Delta g_{N_3}^{Eu,\mathbf{Lk}}$ [kJ mol^{-1}]	7.1(1.2)/−40(7)	7.5(8)/−43 (4)	6.0(5)/−34(3)
$\log(f_{N_2O}^{Eu,\mathbf{Lk}})/\Delta g_{N_2O}^{Eu,\mathbf{Lk}}$ [kJ mol^{-1}]	7.5(1.2)/−43(7)	7.9(8)/−45(5)	6.4(5)/−37(3)
$\log(u^{LL})/\Delta E^{LL}$ [kJ mol^{-1}]	−2.7(1.6)/15(9)	−3.0(8)/17(5)	−1.3(4)/7(3)
$\log(u^{MM})/\Delta E^{MM}$ [kJ mol^{-1}]	−6.7(3.4)/38(19)	−8.4/48	−3.7(9)/21(5)
$\log(c^{eff})/\Delta g_{corr}^{Eu,\mathbf{Lk}}$ [kJ mol^{-1}]	2.1(3.3)/−12(19)	2.7(1.8)/−16(10)	−0.47/2.7

[a] The calculated values of $\log(u^{MM})$ or c^{eff} were blocked during the fitting process (see text). Standard errors estimated by the least-squares fits are given between parentheses. [b] $\log(u^{MM}) = -8.4$. [c] $c^{eff} = 0.34$.

 © 2005 Wiley-VCH Verlag GmbH & Co. KGaA, Weinheim

at the concentrations (10^{-4}–10^{-5} M) used for recording reliable absorption spectra.[2,3,6–10] Therefore, $\log(\beta_{m,n})$ are estimated within ±5–10%, and the quoted errors given in Table 4, indeed refer to those obtained during the nonlinear least-squares fit of the spectrophotometric data.[2,3,6–10] For example, $\log(\beta_{1,3}^{Eu,\mathbf{L2}})=19.4(5)$ must be compared with $\log(\beta_{1,3}^{Sm,\mathbf{L2}})=17.5(4)$ and $\log(\beta_{1,3}^{Gd,\mathbf{L2}})=18.8(5)$ found for the two next neighbours along the lanthanide series, and for which we do not expect any significant change.[8] With this in mind, the average relative discrepancy of 6.4% (4.7% if we neglect $[Eu(\mathbf{L2})_3]^{3+}$, Figure 3) observed between experimental and recalculated constants remains acceptable (Table 4).

The microscopic intermolecular free energies $\Delta g_{N_3}^{Eu}=-RT\ln(f_{N_3}^{Eu})$ and $\Delta g_{N_2O}^{Eu}=-RT\ln(f_{N_2O}^{Eu})$ are identical within experimental errors (Table 5), which contrasts with $\Delta g_{N_3}^{Eu}<\Delta g_{N_2O}^{Eu}$ suggested by using the original site-binding model.[8] In the latter model, the three wrapped strands in $[Eu_m(\mathbf{Lk})_3]^{3m+}$ are considered as a preorganized receptor, which defines an arbitrary zero-level of the free energies. The observed discrepancy with the extended site-binding model discussed here, illustrates the consequences of the explicit consideration of specific intramolecular entropic contributions (c^{eff}) and interligand interactions (u^{LL}) in each microspecies according to Equation (1), which are neglected ($c^{eff}=1$ and $u^{LL}=1$) in the site-binding model.[5,8] The fitted intermetallic interaction energy $\Delta E^{MM}\approx 38\ kJ\,mol^{-1}$ (Table 5) corresponds to the lower limit observed in the related bimetallic helicates $[Ln_2(\mathbf{L2})_3]^{6+}$ (Ln = Ce–Lu).[8] The repulsive interligand interaction $\Delta E^{LL}\approx 15\ kJ\,mol^{-1}$ is diagnostic for a negatively cooperative binding of the strands to the metal ions. Since both interligand and intermetallic repulsion are repulsive (i.e., $\Delta E^{MM}>0$ and $\Delta E^{LL}>0$), the cooperativity indexes $\log(I_c^{MM})$, $\log(I_c^{LL})$, and $\log(I_c^{tot})$ calculated with Equation (28) are systematically negative and point to negatively cooperative assembly processes for these highly charged lanthanide-containing helicates $[Eu_m(\mathbf{Lk})_n]^{3m+}$. Comparisons between the interligand I_c^{LL} and the intermetallic I_c^{MM} contributions to I_c^{tot} indicate that multiligand assemblies are preferred over successive Eu^{III} binding, a feature that may account for the systematic observation of $[Eu(\mathbf{L1})_2]^{3+}$ as the keystep intermediate (instead of $[Eu_2\mathbf{L1}]^{6+}$) in the self-assembly mechanism leading to $[Eu_2(\mathbf{L1})_3]^{6+}$.[10] The large uncertainties affecting c^{eff} prevents its detailed interpretation, but it stimulates us to perform control fits, in which the two extreme theoretical values of $\log(u^{MM})=-8.4$ (model 1)[8] and $c^{eff}=0.34$ (model 2)[14] are alternatively fixed, as previously discussed for Cu–**Lk** helicates. The recalculated formation constants are still satisfying (Table 4), and the fitted parameters roughly span the range of the uncertainties obtained during the global fit (Table 5).

Finally, we have performed an ultimate nonlinear least-squares fit, in which the debatable stability constant $\log(\beta_{1,3}^{Eu,\mathbf{L2}})=19.4(5)$ [Eq. (41)] is neglected (Table 4). Convergence readily occurs without resorting to any constraint concerning $\log(u^{MM})$ and/or c^{eff} (Table S2, Supporting Information), and the eight recalculated stability constants modeled with Equations (34), (36)–(40), and (42)-(43) almost exactly fit the experimental data (Table S3, Supporting Information). Although any reevaluation of experimental data is out of the scope of this contribution, this result indicates that the analysis of the spectrophotometric data implying the complex $[Eu(\mathbf{L2})_3]^{3+}$ should be carefully reconsidered.[8] This suggestion is further supported by the a posteriori estimation of $\log(\beta_{1,3}^{Eu,\mathbf{L2}})=16.2$ obtained by using Equation (41) and the microscopic parameters of Table S2 (Supporting Information), which is in a good agreement with stability constants reported for monometallic complexes $[Ln\mathbf{L}_3]^{3+}$ possessing analogous tridentate N_2O binding sites.[16] Interestingly, ΔE^{MM} and ΔE^{LL} are reduced, but remain positive, which confirms negative cooperative.

Testing the principle of maximum site occupancy in trimetallic helicates displaying a negative cooperative effect: As previously described for the cooperative process leading to $[Eu_m(\mathbf{L3})_n]^{(3m-2n)+}$,[1] we have, a posteriori, estimated the formation constants of selected $[Cu_m(\mathbf{Lk})_n]^{m+}$ and $[Eu_m(\mathbf{Lk})_n]^{3m+}$ complexes, which deviate from the principle of maximum site occupancy (Figure 4).[13] The predicted constants for these unsaturated complexes are indeed 2–4 orders of magnitude smaller (Tables 6 and 7) than those

Table 6. Predicted[a] stability constants for unsaturated $[Cu_m(\mathbf{L4})_n]^{m+}$ complexes.

Species	Type	$\log(\beta_{m,n}^{Cu,\mathbf{L4}})$	Equation	x_i[c]
$[Cu_3(\mathbf{L4})_2]^{3+}$	saturated	18.6	27	>0.999
$[Cu_3(\mathbf{L4})_2]^{3+}$ (A)	unsaturated	15.3	[b]	5.0×10^{-4}
$[Cu_3(\mathbf{L4})_2]^{3+}$ (B)	unsaturated	12.0	[b]	2.5×10^{-7}
$[Cu_3(\mathbf{L4})_2]^{3+}$ (C)	unsaturated	14.1	[b]	3.2×10^{-5}
$[Cu_2(\mathbf{L4})_2]^{2+}$ (ct)	saturated	13.5	13 (26)	0.998
$[Cu_2(\mathbf{L4})_2]^{2+}$ (ct, A)	unsaturated	10.7	[b]	2.0×10^{-3}
$[Cu_2(\mathbf{L4})_2]^{2+}$ (tt)	saturated	13.4	12 (26)	0.992
$[Cu_2(\mathbf{L4})_2]^{2+}$ (tt, A)	unsaturated	11.3	[b]	8.0×10^{-3}

[a] Computed using the fitted parameters in Table 2 ($\log(u^{MM})=-1.8$, model 1). [b] The corresponding equation is given in Figure 4a. [c] Moles fractions calculated with $x_i=\beta_i/\sum_j \beta_j$ (see text).

Table 7. Predicted[a] stability constants for unsaturated $[Eu_m(\mathbf{L6})_n]^{3m+}$ complexes.

Species	Type	$\log(\beta_{m,n}^{Eu,\mathbf{L6}})$	Equation	x_i[c]
$[Eu_3(\mathbf{L6})_3]^{9+}$	saturated	33.9	37	>0.999
$[Eu_3(\mathbf{L6})_3]^{9+}$ (A)	unsaturated	30.8	[b]	7.9×10^{-4}
$[Eu_3(\mathbf{L6})_3]^{9+}$ (B)	unsaturated	27.4	[b]	3.2×10^{-7}
$[Eu_3(\mathbf{L6})_3]^{9+}$ (C)	unsaturated	24.2	[b]	2.0×10^{-10}
$[Eu_3(\mathbf{L6})_3]^{9+}$ (D)	unsaturated	27.5	[b]	4.0×10^{-7}
$[Eu_2(\mathbf{L6})_3]^{6+}$ (ct)	saturated	26.3	20 (36)	>0.999
$[Eu_2(\mathbf{L6})_3]^{6+}$ (ct, A)	unsaturated	23.0	[b]	5.0×10^{-4}
$[Eu_2(\mathbf{L6})_3]^{6+}$ (tt)	saturated	28.1	19 (36)	0.994
$[Eu_2(\mathbf{L6})_3]^{6+}$ (tt, A)	unsaturated	25.9	[b]	6.0×10^{-3}
$[Eu_3(\mathbf{L6})_2]^{9+}$	saturated	25.3	34	0.999
$[Eu_3(\mathbf{L6})_2]^{9+}$ (A)	unsaturated	19.0	[b]	5.0×10^{-7}
$[Eu_3(\mathbf{L6})_2]^{9+}$ (B)	unsaturated	12.2	[b]	7.9×10^{-14}
$[Eu_3(\mathbf{L6})_2]^{9+}$ (C)	unsaturated	22.3	[b]	1.0×10^{-3}

[a] Computed using the fitted parameters in Table 5 (global fit). [b] The corresponding equation is given in Figure 4b. [c] Moles fractions calculated with $x_i=\beta_i/\sum_j \beta_j$ (see text).

© 2005 Wiley-VCH Verlag GmbH & Co. KGaA, Weinheim

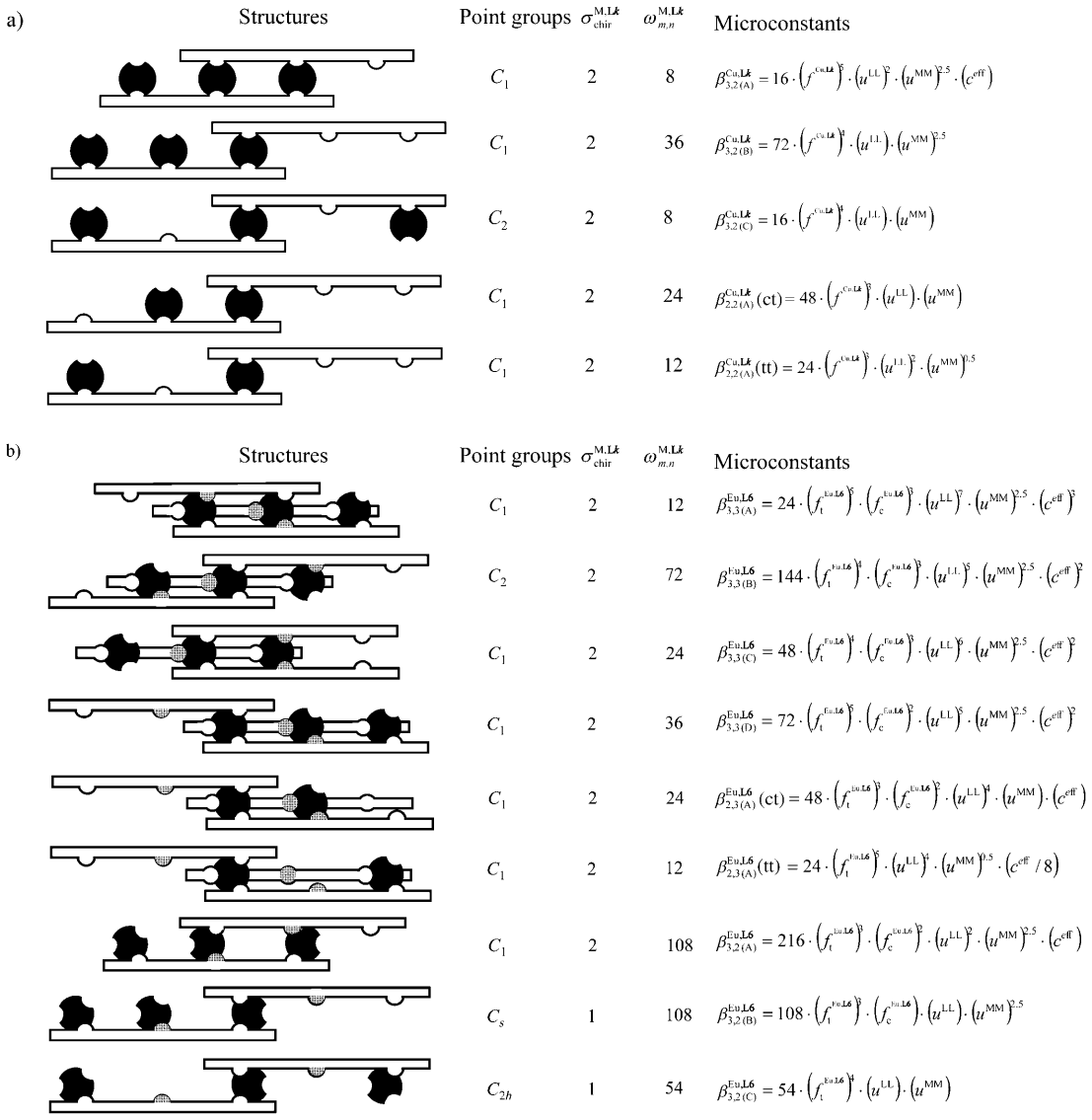

Figure 4. Schematic structures, symmetries, degeneracies and modeled formation constants for selected a) $[Cu_m(\mathbf{L}k)_n]^{m+}$ and b) $[Eu_m(\mathbf{L6})_n]^{3m+}$ microspecies deviating from the principle of maximum site occupancy.

found for the saturated analogues (Tables 1 and 4), which justifies their neglect in our model. However, the free-energy gap between the stability of an unsaturated microspecies and its saturated analogue strongly depends on ΔE^{LL}, because the reduction of the total number of dative bonds in the unsaturated species may be overcome by the parallel decrease of the total interligand repulsion, when considering negatively cooperative processes. We thus predict, that systems exhibiting strong negative cooperativity may escape the principle of maximum site occupancy, a situation not encountered for $[Cu_m(\mathbf{L}k)_n]^{m+}$ and $[Eu_m(\mathbf{L}k)_n]^{3m+}$ because the mole fractions of the saturated species $x^{saturated} = \beta_{m,n}^{unsaturated}/(\Sigma\beta_{m,n}^{unsaturated} + \beta_{m,n}^{saturated})$ are systematically larger than 0.99 (Tables 6 and 7).

Conclusion

The extended site-binding model, compactly formulated in Equation (1), combines the minimal set of microscopic thermodynamic parameters required for the rational modeling of the free-energy change occurring when mixtures of free ligands and metal ions react to give sophisticated self-assembled architectures. Compared to its application to much simpler coordination complexes characterized by ligand strands possessing identical binding sites,[1] the consideration of different sites in the trimetallic $[Cu_3(\mathbf{L}k)_2]^{3+}$ and $[Eu_3(\mathbf{L6})_3]^{9+}$ helicates evidently increases the number of microscopic parameters, but it does not provide major extra difficulties, except for some efforts in obtaining a statistical formalism for the degeneracy factors (see appendix). However, the limited number of accessible experimental macro- or micro-

 © 2005 Wiley-VCH Verlag GmbH & Co. KGaA, Weinheim

constants usually prevents a direct fitting for a single assembly process. This situation holds for the double-stranded helicates $[Cu_3(\mathbf{Lk})_2]^{3+}$, for which theoretical predictions of either intermetallic interaction[8] or effective concentration[14] are used for limiting the number of fitted parameters. When a series of related self-assembly processes, only differing by a stepwise increase in their metallic nuclearity, is accessible, the amount of available experimental data significantly increases, without implying a parallel change in the number of microscopic parameters. Therefore, simultaneous fits appear as attractive solutions for unravelling the self-assembly of sophisticated complexes, as illustrated for the triple-stranded helicates $[Eu_m(\mathbf{Lk})_3]^{3m+}$. Although the original enthusiasm for designing multimetallic (i.e., multicationic) assemblies driven by positive cooperativity[2,3,6] has been already tempered by Ercolani,[4] who concluded that the latter behaviour is probably much rarer than expected, our thorough analysis further strictly limits the occurrence of positive cooperativity to special cases, in which the unavoidable intermetallic repulsion is overcome by some specific electronic changes and/or secondary intramolecular interactions accompanying the ligand binding processes. Such a situation is encountered in the self-assembly of $[Eu_2(\mathbf{L3})_3]$, because 1) the intermetallic repulsion is limited by the charge compensation provided by the multicomplexation of anionic carboxylates to Eu^{3+} and 2) the formation of the multistranded architectures is tightened by a peripheral belt of favorable interstrand interactions.[1] These conditions are not met for the larger assemblies $[Cu_3(\mathbf{Lk})_2]^{3+}$ and $[Eu_3(\mathbf{L6})_3]^{9+}$, and both intermetallic and interligand interactions are repulsive.

Finally, the application of this simple extended site-binding model is not limited to zero-dimensional monometallic complexes, or one-dimensional multimetallic helicates. Two-dimensional arrays of metal ions connected by bi-dimensional ligands,[17] and three-dimensional systems, pertinent to cages or clusters, can be easily amenable to modeling, according that their thermodynamic stabilities are available.[18]

Appendix

Calculation of the degeneracy $\omega_{m,n}$ for each microspecies contributing to a specific macrospecies $[Cu_m(\mathbf{Lk})_n]^{m+}$: For each ligand strand in a specific microspecies, the m metal ions are distributed either 1) with one metal occupying the central site (characterized by the microscopic affinity $(f_c^{Cu,\mathbf{Lk}})$ and $m-1$ metals lying in the remaining terminal sites (characterized by the total microscopic affinity $(f_t^{Cu,\mathbf{Lk}})^{m-1}$; or 2) with the m metal ions exclusively occupying the terminal sites (characterized by the total microscopic affinity $(f_t^{Cu,\mathbf{Lk}})^m$. The degeneracies of the microspecies $\omega_{m,n}$(micro) contributing to a specific macrospecies $[Cu_m(\mathbf{Lk})_n]^{m+}$ are thus given by the coefficients of the binomial distribution shown in Equation (44), whereby $p^c=1$, $p^t=2$, and $f_c^{Cu,\mathbf{Lk}}$ and $f_t^{Cu,\mathbf{Lk}}$ are the arguments of the function.

$$(C_n^v)^m[(C_1^{p^c}C_{m-1}^{p^t})f_c^{Cu,\mathbf{Lk}}(f_t^{Cu,\mathbf{Lk}})^{m-1}+(C_0^{p^c}C_m^{p^t})(f_c^{Cu,\mathbf{Lk}})^0(f_t^{Cu,\mathbf{Lk}})^m]^n \quad (44)$$

A straightforward mathematical development transforms Equation (44) into Equation (45),[19] which can be used for calculating the degeneracy of each specific microspecies characterized by its complete microscopic affinity argument.

$$(C_n^v)^m\sum_{i=0}^{n}\{C_i^n[(C_1^{p^c}C_{m-1}^{p^t})f_c^{Cu,\mathbf{Lk}}(f_t^{Cu,\mathbf{Lk}})^{m-1}]^i[(C_0^{p^c}C_m^{p^t})(f_t^{Cu,\mathbf{Lk}})^m]^{n-i}\} \quad (45)$$

Finally, since $\omega_{m,n}$(macro)$=\Sigma\omega_{m,n}$(micro), the consideration of the binomial coefficients of Equation (45) leads to Equation (46), which highlights how the total degeneracy of the macrospecies is partitioned between its contributing microspecies.

$$\omega_{m,n}(\text{macro})=(C_n^v)^m(C_m^p)^n=(C_n^v)^m\sum_{i=0}^{n}\{C_i^n(C_1^{p^c}C_{m-1}^{p^t})^i(C_0^{p^c}C_m^{p^t})^{n-i}\} \quad (46)$$

Let's illustrate the use of Equation (45) for calculating the degeneracy of the microspecies contributing to the $[Cu_2(\mathbf{Lk})_2]^{2+}$ macrospecies ($m=2$, $n=2$, $v=2$, $p=3$) . Its total degeneracy $(C_n^v)^m(C_m^p)^n=(C_2^2)^2(C_2^3)^2=9$, is partitioned between $n+1=3$ microspecies. Application of Equation (45) gives Equation (47), the eventual development of which is summarized in Equation (48).

$$(C_2^2)^2\sum_{i=0}^{2}\{C_i^2[(C_1^1C_1^2)(f_c^{Cu,\mathbf{Lk}}f_t^{Cu,\mathbf{Lk}})]^i[(C_0^1C_2^2)(f_t^{Cu,\mathbf{Lk}})^2]^{2-i}\} \quad (47)$$

$$1(f_t^{Cu,\mathbf{Lk}})^4+4(f_c^{Cu,\mathbf{Lk}})(f_t^{Cu,\mathbf{Lk}})^3+4(f_c^{Cu,\mathbf{Lk}})^2(f_t^{Cu,\mathbf{Lk}})^2 \quad (48)$$

The argument $(f_t^{Cu,\mathbf{Lk}})^4$ of the first term in Equation (48) corresponds to the microspecies, in which the four terminal binding sites of the two ligands are occupied, and we consequently safely assign its coefficient to $\omega_{2,2}(\text{tt})=1$ (Figure 2). The argument $(f_c^{Cu,\mathbf{Lk}})(f_t^{Cu,\mathbf{Lk}})^3$ of the second term in Equation (48) corresponds to the constrained structure, in which the two terminal sites of one ligand are connected to the two adjacent central and terminal sites of the second ligand ($\omega_{2,2}$(constrained)$=4$). This species is excluded from our model, because the rigidity of the ligand strand prevents such arrangement. Finally, the last term of Equation (48) corresponds to the microspecies in which two central and two terminal binding sites are connected to Cu^I. We thus attribute $\omega_{2,2}(\text{ct})=4$ (Figure 2), and eventually verify that the sum of the degeneracies of the microspecies ($1+4+4=9$) indeed matches the degeneracy of the macrospecies $[Cu_2(\mathbf{Lk})_2]^{2+}$ [Eq. (46)]. The appropriate degeneracy factors have been calculated for all microspecies, and shown in Figure 2.

Experimental Section

Computational details: Computing of thermodynamic parameters were performed by using linear and non-linear regression methods with least-squares minimisation included in the Excel© and Mathematica®5 programs.

Acknowledgement

This work was supported through grants of the Swiss National Science Foundation.

[1] J. Hamacek, M. Borkovec, C. Piguet, *Chem. Eur. J.* **2005**, *11*, 10.1002/chem.200500290.
[2] A. Pfeil, J.-M. Lehn, *J. Chem. Soc. Chem. Commun.* **1992**, 838.
[3] a) N. Fatin-Rouge, S. Blanc, A. Pfeil, A. Rigault, A. M. Albrecht-Gary, J.-M. Lehn, *Helv. Chim. Acta* **2001**, *84*, 1694; b) A. Marquis-Rigault, Ph.D. Thesis, Université Louis Pasteur, Strasbourg (France), **1992**.
[4] a) G. Ercolani, *J. Am. Chem. Soc.* **2003**, *125*, 16097; b) G. Ercolani, *J. Phys. Chem. B* **2003**, *107*, 5052.

© 2005 Wiley-VCH Verlag GmbH & Co. KGaA, Weinheim

[5] C. Piguet, M. Borkovec, J. Hamacek, K. Zeckert, *Coord. Chem. Rev.* **2005**, *249*, 705.
[6] S. Floquet, N. Ouali, B. Bocquet, G. Bernardinelli, D. Imbert, J.-C. G. Bünzli, G. Hopfgartner, C. Piguet, *Chem. Eur. J.* **2003**, *9*, 1860.
[7] S. Floquet, M. Borkovec, G. Bernardinelli, A. Pinto, L.-A. Leuthold, G. Hopfgartner, D. Imbert, J.-C. G. Bünzli, C. Piguet, *Chem. Eur. J.* **2004**, *10*, 1091.
[8] K. Zeckert, J. Hamacek, J.-P. Rivera, S. Floquet, A. Pinto, M. Borkovec, C. Piguet, *J. Am. Chem. Soc.* **2004**, *126*, 11589.
[9] C. Piguet, J.-C. G. Bünzli, G. Bernardinelli, G. Hopfgartner, A. F. Williams, *J. Am. Chem. Soc.* **1993**, *115*, 8197.
[10] J. Hamacek, S. Blanc, M. Elhabiri, E. Leize, A. van Dorsselaer, C. Piguet, A. M. Albrecht-Gary, *J. Am. Chem. Soc.* **2003**, *125*, 1541.
[11] H. Jacobson, W. H. Stockmayer, *J. Chem. Phys.* **1950**, *18*, 1600.
[12] R. J. Motekaitis, A. E. Martell, R. A. Hancock, *Coord. Chem. Rev.* **1994**, *133*, 39.
[13] a) R. Krämer, J.-M. Lehn, A. Marquis-Rigault, *Proc. Natl. Acad. Sci. USA* **1993**, *90*, 5394; b) J.-M. Lehn, A. V. Eliseev, *Science* **2001**, *291*, 2331.
[14] J. M. Gargano, T. Ngo, J. Y. Kim, D. W. K. Acheson, W. J. Lees, *J. Am. Chem. Soc.* **2001**, *123*, 12909.
[15] C. Galli, L. Mandolini, *Eur. J. Org. Chem.* **2000**, 3117.
[16] T. Le Borgne, P. Altman, N. André, J.-C. G. Bünzli, G. Bernardinelli, P.-Y. Morgantini, J. Weber, C. Piguet, *Dalton Trans.* **2004**, 723.
[17] D. Chapon, C. Husson, P. Delangle, C. Lebrun, P. J. A. Vottéro, *J. Alloys Compd.* **2001**, *323–324*, 128.
[18] a) D. L. Caulder, K. N. Raymond, *Acc. Chem. Res.* **1999**, *32*, 975; b) J.-M. Lehn, *Chem. Eur. J.* **2000**, *6*, 2097; c) D. P. Funeriu, J.-M. Lehn, K. M. Fromm, D. Fenske, *Chem. Eur. J.* **2000**, *6*, 2103; d) D. L. Caulder, C. Brückner, R. E. Powers, S. König, T. N. Parac, J. A. Leary, K. N. Raymond, *J. Am. Chem. Soc.* **2001**, *123*, 8923; e) T. Yamaguchi, S. Tashiro, M. Tominaga, M. Kawano, T. Oseki, M. Fujita, *J. Am. Chem. Soc.* **2004**, *126*, 10818.
[19] For a mathematical background concerning the binomial theorem see for example, http://mathworld.wolfram.com.

Received: March 15, 2005
Published online: June 30, 2005

 © 2005 Wiley-VCH Verlag GmbH & Co. KGaA, Weinheim